

1 Title: Niche partitioning of methane-oxidizing bacteria along the
2 oxygen-methane counter gradient of stratified lakes

3 Running title: Methanotrophs in the oxygen-methane counter gradient

4 Magdalena J. Mayr^{1,2}, Matthias Zimmermann^{1,2}, Carole Guggenheim², Andreas Brand^{1,2}, Helmut
5 Bürgmann¹

6 ¹Department of Surface Waters—Research and Management, Eawag, Swiss Federal Institute of
7 Aquatic Science and Technology, Kastanienbaum, Switzerland

8 ²Institute of Biogeochemistry and Pollutant Dynamics, Department of Environmental Systems
9 Science, ETH Zurich, Swiss Federal Institute of Technology, Zurich, Switzerland

10 *Corresponding author: Magdalena J. Mayr, Seestrasse 79, 6047 Kastanienbaum, +41 58 765 2142,
11 magdalena.mayr@eawag.ch

This document is the accepted manuscript version of the following article:
Mayr, M. J., Zimmermann, M., Guggenheim, C., Brand, A., & Bürgmann, H. (2019).
Niche partitioning of methane-oxidizing bacteria along the oxygen-methane counter
gradient of stratified lakes. ISME Journal. <https://doi.org/10.1038/s41396-019-0515-8>

12 Abstract

13 Lakes are a significant source of atmospheric methane, although methane-oxidizing bacteria
14 consume most methane diffusing upward from anoxic sediments. Diverse methane-oxidizing bacteria
15 form an effective methane filter in the water column of stratified lakes, yet, niche partitioning of
16 different methane-oxidizing bacteria along the oxygen-methane counter gradient remains poorly
17 understood. In our study, we reveal vertical distribution patterns of active methane-oxidizing
18 bacteria along the oxygen-methane counter gradient of four lakes, based on amplicon sequencing
19 analysis of 16S rRNA and *pmoA* genes, and 16S rRNA and *pmoA* transcripts, and potential methane
20 oxidation rates. Differential distribution patterns indicated that ecologically different methane-
21 oxidizing bacteria occupied the methane-deficient and oxygen-deficient part above and below the
22 oxygen-methane interface. The interface sometimes harbored additional taxa. Within the dominant
23 *Methylococcales*, an uncultivated taxon (CABC2E06) occurred mainly under methane-deficient
24 conditions, whereas *Crenothrix*-related taxa preferred oxygen-deficient conditions. *Candidatus*
25 *Methylomirabilis limnetica* (NC10 phylum) abundantly populated the oxygen-deficient part in two of
26 four lakes. We reason that the methane filter in lakes is structured and that methane-oxidizing
27 bacteria may rely on niche-specific adaptations for methane oxidation along the oxygen-methane
28 counter gradient. Niche partitioning of methane-oxidizing bacteria might support greater overall
29 resource consumption, contributing to the high effectivity of the lacustrine methane filter.

30 Introduction

31 Methane is responsible for about 20% of the warming induced by long-lived greenhouse gases since
32 preindustrial times [1]. Freshwater lakes significantly add to the natural global methane emissions [2,
33 3]. On the other hand methane-oxidizing bacteria (MOB) greatly reduce methane emissions from
34 lakes to the atmosphere [4]. Typically, many MOB taxa co-occur in lake water columns [5], although
35 all rely on the same primary resources, methane and oxygen, for growth. This raises the question of
36 how diversity within this functional group is maintained or how the “competitive exclusion principle”
37 [6] is bypassed. Niche partitioning could be one possible explanation for the observed diversity [7],
38 and might further be a mechanism that increases the efficiency [8] of the methane filter in lakes.

39 Lacustrine MOB usually belong to *Alpha*- or *Gammaproteobacteria*, which oxidize methane with
40 oxygen [9]. However, high abundance of *Candidatus* Methylomirabilis limnetica (NC10 phylum) has
41 recently been reported in a lake water column [10]. *Candidatus* Methylomirabilis limnetica likely uses
42 an intra-aerobic pathway for methane oxidation, forming oxygen from nitrite like *Ca.*
43 *Methylomirabilis oxyfera* [11]. Other anaerobic methane oxidizers, i.e. ANME or related archaea [12–
44 14], were found in lake sediments [15, 16], but seem to be of minor importance in anoxic water
45 columns [17, 18]. Although the coarse phylogenetic affiliation of lacustrine MOB is known, several
46 uncultivated lake and aquatic clusters within type Ia and Ib MOB (*Gammaproteobacteria*) are defined
47 solely based on environmental *pmoA* sequences [9, 19]. Sequencing of *pmoA* is widely used for MOB
48 detection in the environment [20]. However, the ecology and relevance of many uncultivated MOB
49 remain largely unknown.

50 The oxygen-methane counter gradient of stratified lakes potentially provides distinct niches for MOB:
51 methane-deficient conditions with excess oxygen, oxygen-deficient conditions with methane in
52 excess, and a narrow interface with possibly unlimited resource supply (Figure 1). MOB diversity and
53 efficient methane filtering from stratified lakes may depend on niche adaptations of MOB to ambient
54 oxygen and methane concentrations. Previous studies indeed indicated vertical shifts in lacustrine

55 MOB assemblages below genus level resolution [5, 21, 22]. Although the oxygen-methane interface is
56 generally considered as the main site of methane oxidation, MOB have been shown to be present
57 and active in oxygen-deficient water layers [23]. Fermentation and denitrification serve as oxygen-
58 saving strategies in some isolates [24–26]. Further, oxygen availability has been shown to impact
59 MOB species assemblage in incubations [27]. Isolates are known to have different affinities for
60 methane [28], and in soils different subsets of MOB became active, depending on the supplied
61 methane concentration [29]. In lakes, the oxygen-methane counter gradient is sometimes
62 accompanied by a temperature gradient which might as well act on the MOB assemblage [30].
63 Additionally, other resources like nitrogen or grazing might play a role in structuring MOB niches [31].
64 Despite the evidence for MOB adaptations to resource availability, niche partitioning has not been
65 demonstrated for lacustrine MOB.

66 In this study we investigated to what extent niche partitioning of MOB occurs along the natural
67 oxygen-methane counter gradient in four stratified lakes in order to better understand MOB diversity
68 and the structure of the effective methane filter in lakes. We focused on the section of the water
69 column with oxygen and methane gradients above and below the oxygen-methane interface in these
70 lakes to systematically resolve changes in the MOB assemblage and their potential activity. We
71 compared MOB distribution patterns based on 16S rRNA and rRNA gene, as well as *pmoA* DNA and
72 mRNA sequencing. By correlating MOB distribution patterns to oxygen, methane and temperature,
73 we were able to assign tentative niches to several lacustrine MOB at ASV (amplicon sequence
74 variant) level, including uncultivated MOB.

75 Materials and Methods

76 *Sample collection and physico-chemical lake profiling*

77 We selected four eutrophic Swiss lakes known to accumulate methane in the hypolimnion. Two
78 representatives of two common stratified lake types, seasonally and permanently stratified, were
79 chosen. Seasonally stratified Rotsee [32] (16 m max. depth) and Greifensee [33] (18 m max. depth)

were sampled during stratification on July 27th and August 20th 2015, respectively. Permanently stratified Lake Zug (198 m max. depth) and Lake Lugano (288 m max. depth) [34] were sampled October 12th and November 4th 2015, respectively. Temperature, oxygen and pressure were profiled with a custom-made *in situ* analyzer (PIA) [34], equipped with a remote-controlled 50 mL syringe rosette sampler. PIA enabled sampling of steep gradients, if necessary. Compared to commonly used Niskin bottles (depth integration >50 cm), PIA integrates <5 cm allowing a vertical sampling resolution of 25 cm. Steepness and depth extension of the oxygen-methane gradient differ between lakes. To cover similar concentration ranges vertical spacing of samples was adapted for each lake. Sampling depths were chosen on-site based on preliminary oxygen profiles from two micro-optodes (PSt1 and TOS7, Presens, Regensburg, Germany), the latter with a detection limit down to about 20 nmol L⁻¹ [34].

Water samples for nitrate, nitrite, ammonium, sulfate and dissolved inorganic carbon (DIC) analyses were pre-filtered with a cellulose acetate filter (0.2 µm pore size, Sartorius, Göttingen, Germany) and stored at 4°C until analysis. Nitrate and nitrite were quantified with flow-injection analysis (ISO 13395, SAN++, Skalar, Breda, The Netherlands), sulfate with ion chromatography (881 IC compact plus, Metrohm, Herisau, Switzerland) and DIC and non-purgeable organic carbon with a total organic carbon analyzer (TOC-L, Shimadzu, Kyoto, Japan). Nitrite was measured in Rotsee, Greifensee and Lake Zug. Ammonium was measured photometrically according to [35]. For a summary of environmental parameters, see Supplementary Table 1.

For methane measurements 20 ml lake water was filled into sealed 40 ml serum bottles and methane concentrations were derived from headspace concentrations measured by gas chromatography. Details are provided in the supplementary methods.

Potential methane oxidation rates

We used a modified protocol [17, 36] to measure potential methane oxidation rates by incubations with ¹³C-CH₄ and oxygen. Rates were calculated from the linear increase of ¹³C-CO₂ over five time points (0, 3, 9, 21, 44 hours). Details are provided in the supplementary methods.

Nucleic acid preparation

Immediately after sampling, we filtered 110-220 ml of lake water onto 0.2 µm pore size cellulose acetate filters (Sartorius) and froze them on dry ice. Filters were stored at -80°C until extraction. DNA and RNA were extracted simultaneously with the AllPrep DNA/RNA Mini Kit (Qiagen, Hilden, Germany) with bead beating (glass beads: 150-212 µm) on a FastPrep-24 homogenizer (45sec, step 5, MP Biomedicals, Santa Ana, CA, USA). Residual DNA from the RNA was removed with the Ambion TURBO DNA-free Kit (Thermo Fisher Scientific, Waltham, MA, USA), which was checked by 16S rRNA gene PCR (27f/1492r, 35 cycles) and gel electrophoresis. If necessary, we repeated the DNA removal step. RNA was reverse-transcribed with random hexamers into cDNA with the SuperScript IV First-Strand Synthesis System (Invitrogen, Thermo Fisher Scientific), which was further used for 16S rRNA and *pmoA* mRNA library preparation.

Library preparation and sequencing

Sequencing of 16S rRNA gene was used to identify MOB within their well-described phylogenetic clades and to estimate their relative abundance within the bacterial community. Reverse transcribed rRNA was used to verify protein synthesis potential. The commonly used functional marker gene *pmoA* [9], encoded by most MOB provided an independent assessment of the assemblage and its mRNA provided further information on MOB activity. The 16S rRNA gene/rRNA and *pmoA* DNA/mRNA amplicon libraries were sequenced in two runs on an Illumina MiSeq platform (Illumina Inc., San Diego, CA, USA) with 600-cycle MiSeq reagent kit v3 (Illumina Inc.) at the Genetic Diversity Centre (ETH Zurich) to obtain >10000 reads per sample. PCR conditions and library preparation are detailed in the supplementary methods.

Sequence analyses

We used the DADA2 workflow (version 1.6.0) [37] in R (3.4.2) [38] to determine amplicon sequence variants (ASVs) of *pmoA* genes and their mRNA transcripts, and 16S rRNA genes and 16S rRNA [39]. *pmoA* ASVs were translated to amino acid sequences (aaASVs) in MEGA7 [40], and aaASVs reaching >2% relative abundance in at least one sample of the respective lake were retained. 16S rRNA ASVs

were classified based on the SILVA database (v132) [41]. ASVs affiliated with known methanotrophic groups (Order *Methylococcales*, Genus *Methylocystis*, Genus *Candidatus Methyloirabilis*) were used for further analyses if reaching >0.2% relative abundance in at least two samples of the respective lake. Phylogenetic trees of MOB 16S rRNA gene and *pmoA* mRNA were calculated with MEGA7 neighbor-joining method using Jukes-Cantor evolutionary distance or Poisson correction method, respectively, and 10000 bootstrap replications. Details on the amplicon sequence analysis are provided in the supplementary methods.

Sequence accession numbers

Raw reads were submitted to the European Nucleotide Archive under project number PRJEB27579.

Quantitative real-time PCR

Copy numbers of *pmoA* genes and transcripts were quantified with qPCR in a 10 µl volume using SYBR Green I Master chemistry (Roche Diagnostics, Rotkreuz, Switzerland) with 0.2 µM primer (189f, mb661) [42] and 2 µl of 1:10 diluted DNA or cDNA on a LightCycler 480 (Roche). The cycling program of [43] was adapted by using 10 min initial denaturation, 15 s denaturation during cycling and data acquisition at 79 °C. The standard, a plasmid containing the *pmoA* gene of *Methylococcus capsulatus* was measured in quadruplicates at eight different dilutions (5×10^7 to 5 copies per reaction). Samples were run in triplicate and quantified by means of the second derivative maximum analysis method of the LightCycler 480 software (version 1.5.1.62).

Statistical analyses

Depth distributions of relative abundance of ASVs and aaASVs, normalized to maximum abundance in the profile, were hierarchically clustered based on Pearson's distance using pvclust package (2.0.0) in R (3.5.0), UPGMA agglomeration and 10000 bootstrap replications. Clusters representing similar depth distribution were assigned based on a distance threshold individually chosen for each lake. All clusters have a reasonable bootstrapping support of AU *p*-values ≥80% (AU, approximately unbiased *p*-values [44]). Venn diagrams showing taxon overlap between lakes were created with the

VennDiagram package (1.6.18) in R [45]. Unconstrained detrended correspondence analysis (DCA) of MOB 16S rRNA gene ASVs by lake with samples colored by niche is shown in Supplementary Figure S1. Spearman correlation p -values were corrected for multiple testing [46].

Canonical correspondence analysis (CCA) was conducted to show preferences of MOB along the gradients of oxygen, methane, and temperature across all four lakes and to test the explanatory power of the variables linked to our niche hypothesis. Constrained axes were significant ($p < 0.001$, `anova.cca`, `vegan` [47]). Sample scores are shown in Supplementary Figure S2. For its ability to handle linear and unimodal taxa distributions CCA was chosen. The CCAs were performed with `phyloseq` [48] (1.24.2) in R, based on Chi-square dissimilarity matrix of relative abundances (sample sum=1), and centered and scaled physicochemical variables (values <LOQ set to zero). Additional to this hypothesis-driven CCA, a CCA was performed based on a subset of environmental variables (temperature, oxygen, methane, nitrate and sulfate concentration, Supplementary Figure S3) curated from available environmental variables by forward selection and removal of variables with a variance inflation factor above ten. Details are provided in the supplementary methods.

Results

Oxygen-methane counter gradients and definition of potential MOB niches

In all four lakes we found vertical oxygen-methane counter gradients; oxygen decreased with depth, whereas methane increased in the oxygen-deficient part (Figure 2a). The oxygen-methane counter gradients sampled spanned different concentration ranges, the smallest being in Lake Zug (max. 37 $\mu\text{mol L}^{-1}$ O_2 and max. 4 $\mu\text{mol L}^{-1}$ CH_4) followed by Greifensee and Lake Lugano. The largest range was found in Rotsee with up to 400 $\mu\text{mol L}^{-1}$ oxygen and up to 228 $\mu\text{mol L}^{-1}$ methane – the only case with a distinct oxygen-methane overlap at the interface (Figure 2a, Rotsee). Vertical extension and steepness of the gradients varied between lakes, therefore we sampled over 4.25 m in Rotsee (25 cm resolution), 7.2 m in Greifensee (40 cm resolution), 40 m in Lake Zug (2 or 4 m resolution) and 80 m in Lake Lugano (8 m resolution). Temperature profiles are shown in Supplementary Figure S4.

Potential niches were defined based on differential resource availability. A methane-deficient but excess oxygen niche (orange, Figure 2) was defined as the part of the gradient from the shallowest sample to the depth where either oxygen dropped below $1 \mu\text{mol L}^{-1}$ (dashed line) or methane concentrations started to increase relative to samples above (Rotsee). Methane generally did not exceed $\sim 1 \mu\text{mol L}^{-1}$. An oxygen-deficient and excess methane niche (blue) was designated where oxygen was below $1 \mu\text{mol L}^{-1}$ and methane levels increased relative to samples above. The interface in between these main zones varied in its characteristics: In Rotsee oxygen and methane overlapped at concentrations $>1 \mu\text{mol L}^{-1}$ (green). In contrast, in the other lakes we observed a methane-oxygen gap with undetectable or very low concentrations ($<1 \mu\text{mol L}^{-1}$) of both substrates (gray). The proposed niches have internal gradients in substrate concentrations and therefore cannot be considered as internally homogeneous habitats.

Analysis of MOB diversity by 16S rRNA gene sequencing

To identify and study MOB in the context of the general bacterial community, we first used bacterial 16S rRNA gene sequencing. This approach revealed that MOB ASVs affiliated with *Methylococcales* (*Gammaproteobacteria*) were present in all investigated lake samples, whereas *Ca. Methyloirabilis limnetica* (NC10 phylum) was only detected in Lake Zug and Lake Lugano samples (Figure 2b). Summing the ASVs of both clades, the maximum relative abundance of MOB reached at a specific depth was 11% in Rotsee, 15% in Greifensee, 21% in Lake Zug and 26% in Lake Lugano. Between lakes, both unique and shared ASVs occurred (Figure 3a).

Type Ia *Methylococcales* dominated the MOB assemblage. However, the clade consisted of 30 ASVs of several distinct genera (Figure 4a), whose relative abundance varied considerably between different lakes and depths (Figure 2c). Only Greifensee additionally harbored one type Ib *Methylococcales* (ASV_1566, Figure 4a). Alphaproteobacterial MOB sequences occasionally occurred in the raw data, but never exceeded filtering thresholds. ASV_18 with 100% sequence identity to *Ca. Methyloirabilis limnetica* reached up to 6 and 11% of 16S rRNA gene reads in Lake Zug and Lugano, respectively (Figure 2b). Currently known *Ca. Methyloirabilis* require nitrite to oxidize methane [11,

49]. Nitrite exceeded the limit of quantification (LOQ, $0.4 \mu\text{mol L}^{-1}$) at three depths in Lake Zug, but we do not have measurements for Lake Lugano (Figure 2a, Supplementary Table 1). Nitrate concentrations decreased with depth in Lake Zug and Lake Lugano, in the latter falling below LOQ ($<4 \mu\text{mol L}^{-1}$) in the oxygen-deficient part (Figure 2a). Hence, nitrate-reducing microorganisms might provide nitrite.

Depth distribution and niche preference of MOB ASVs

We next analyzed the depth distribution of the identified MOB ASVs along the oxygen-methane counter gradient in each lake. Hierarchical clustering of the depth distributions (relative abundance normalized to the maximum value) based on Pearson's distance revealed groups of ASVs differing with respect to their distribution pattern along the counter gradient and width of their distribution, both indicating niche partitioning. Distribution patterns that conform to preferences for the potential niches can be found in all lakes (Figure 2d). For example, in Rotsee the relative abundance of groups represented by ASV_5, ASV_35, ASV_8 and ASV_4 (Figure 2c, Rotsee) each showed a broad, roughly unimodal distribution with depth. However, the maximum and bulk of the respective distributions centered on the methane-deficient part of the counter gradient (ASV_5), the interface with the oxygen-methane overlap (ASV_35), the interface and below (ASV_8), and the oxygen-deficient part (ASV_4), respectively. Notably, ASV_166 and ASV_98 in Rotsee showed a very narrow distribution restricted to the interface (Supplementary Figure S5). Taxa peaking in the interface were also observed in the other lakes without overlapping methane and oxygen, but these were not interface exclusive. In contrast, several ASVs in Lake Zug did not show a clearly defined abundance maximum or trend (ASV_39, ASV_67, ASV_4, ASV_15, Figure 2c).

Analysis of potentially active MOB by 16S rRNA sequencing

According to the above analysis, MOB occurred throughout the counter gradient, including parts with low resource concentrations, raising questions regarding the metabolic state of these populations. We therefore applied 16S rRNA amplicon sequencing to RNA extracted simultaneously with DNA to assess protein synthesis potential [50]. The depth distributions of MOB rRNA ASVs appeared highly

similar to the rRNA gene analysis presented above (Figure 2c, Supplementary Figure S5 and S6), reflected by a strong correlation of summed up 16S rRNA gene and rRNA MOB relative abundances in each lake (Spearman's $\rho=0.73-0.99$, $p<0.001$, Table 1). Likewise, significant correlations were found between rRNA gene and rRNA based relative abundances of individual MOB ASVs in each lake (Spearman's $\rho=0.88-0.95$, $p<0.001$). This indicates that the observed MOB maintain the protein synthesis potential and are potentially active.

Linking transcriptionally active MOB and potential methane oxidation rates

Further confirmation of activity was sought from analysis of transcriptionally active MOB. For this purpose, we analysed *pmoA* mRNA by subjecting cDNA obtained from RNA extracts of all samples to high-throughput *pmoA* amplicon analysis. Sequence variants of *pmoA* mRNA translated into 30 distinct amino acid amplicon sequence variants (aaASV) that exceeded the 2% abundance threshold. Confirming the 16S rRNA gene and rRNA results, sequences affiliated with type Ia *Methylococcales* were dominant and diverse, with 29 aaASVs (Figure 4b). In accordance with the 16S rRNA gene results, a type Ib aaASV occurred in Greifensee (aaASV22, Figure 4). The primers we used for sequencing and qPCR targeted proteobacterial *pmoA*; therefore, the *pmoA* of *Ca. Methyloiridis* limnetica was not detected.

Similar to 16S rRNA gene and rRNA results, depth distribution profiles of *pmoA* mRNA aaASVs clustered into differential patterns (Figure 5a, b), indicating that these populations actively transcribed *pmoA*. The mostly broad depth distribution of MOB populations with different depth maxima, alongside clusters with narrower depth distribution was likewise confirmed (Figure 5b). For instance, in Rotsee aaASV1 (Figure 5b) dominated from 8 - 9 m depth in the methane-deficient part, similar to ASV_5 (Figure 2c). The distribution of aaASV2 (Figure 5b) at the oxygen-methane interface in Rotsee resembled the distribution of ASV_35 (Figure 2c), indicating transcriptional activity at the interface.

To support the link between *pmoA* transcript abundance and methane oxidation activity we compared them in each lake (Figure 5c). All samples, except for the shallowest measured depth in

Lake Lugano, contained *pmoA* transcripts as detectable by qPCR. Potential methane oxidation rates were significantly correlated with *pmoA* mRNA copies L⁻¹ in all lakes ($p < 0.05$), except Lake Lugano (Table 1). Similarly, MOB 16S rRNA gene relative abundance was significantly correlated with potential methane oxidation rates in all lakes ($p < 0.001$), except Lake Lugano (Table 1). Taken together the data indicate that the observed depth distributions of both 16S rRNA gene MOB ASVs and *pmoA* mRNA aaASVs largely reflect the potentially active MOB assemblage, with the possible exception of the situation in Lake Lugano.

To see if *pmoA* transcripts deviated from gene abundance, we additionally investigated *pmoA* diversity and copy numbers at the DNA level. Gene copies of *pmoA* correlated only in Rotsee and Greifensee with potential methane oxidation rates ($p < 0.01$, Table 1). Distribution patterns of *pmoA* mRNA and DNA aaASVs were however remarkably similar overall (Supplementary Figure S7, S8), with some noteworthy exceptions in Lake Zug and Lugano. In Lake Zug, aaASV1 and aaASV16 showed a *pmoA* transcript maximum at 120 m coinciding with a peak in potential methane oxidation that is not reflected in the *pmoA* gene distribution (Figure 5, Supplementary Figure S7, S8). This suggests that in some cases increased transcriptional activity (*pmoA* mRNA) and not increased abundance (*pmoA* DNA) may have contributed to the observed methane oxidation activity peaks. In Lake Lugano, several aaASVs likewise showed a mismatch between DNA and mRNA (e.g. aaASV13, aaASV1, aaASV2). Most conspicuously, aaASV2 gene increased with depth, whereas its transcripts decreased, indicating decoupling of presence and activity.

General patterns of 16S rRNA gene and pmoA mRNA-based MOB assemblage across lakes

Canonical correspondence analyses (CCA) were conducted to show preferences of MOB along the gradients of oxygen, methane, and temperature across all four lakes and to test the explanatory power of the variables linked to our niche hypothesis, therefore other factors were not included. The CCAs explained 47% and 39% (three significant axes) of the variance in 16S rRNA gene and *pmoA* mRNA data, respectively, revealing general preferences of ASVs and aaASVs along the oxygen-methane gradient in agreement with our hypothesis (Figure 6).

In the following, we focus on taxa occurring in more than one lake. The CCA of 16S rRNA gene ASVs revealed that ASV_5 of the uncultivated CABC2E06 clade correlated most positively to increased oxygen concentration and temperature (Figure 6a). Following the oxygen gradient, ASV_98 and ASV_166 correlated with oxygen, though to a lesser extent, which is in line with the observation that these ASVs occurred at or near the oxygen-methane interface. The majority of MOB ASVs clustered together in the oxygen-deficient, low temperature part of the biplot, indicative of a preference for the oxygen-deficient part of the counter gradient. This group included *Ca. Methyloirabilis limnetica* (ASV_18) and ASV_203, sequence identical to lacustrine Crenothrix. Both ASVs occurred in Lake Zug and Lugano, which contained low to moderate methane concentrations of up to 4 and 39 $\mu\text{mol L}^{-1}$, respectively (Figure 2a). Although ASV_8, related to lacustrine Crenothrix, was mainly present in the oxygen-deficient part, it correlated with methane.

The CCA of *pmoA* mRNA aaASVs confirmed that few MOB taxa correlated with oxygen (Figure 6b). One of them, aaASV1 of the uncultivated Lake cluster 1, occurred in all lakes, like ASV_5 (Figure 6a), and might therefore originate from the same organism. Five aaASVs found exclusively in Greifensee and aaASV6 strongly correlated with oxygen and temperature (Figure 6b). Similar to ASV_166, aaASV16 appeared at intermediate oxygen levels (Figure 6b). In line with the 16S rRNA gene CCA, the *pmoA* mRNA CCA showed that the majority of aaASVs preferentially occurred in oxygen-deficient, low temperature samples (Figure 6b). One of them, aaASV14, is sequence identical to *pmoA* of lacustrine Crenothrix and therefore probably originated from the same organism as 16S rRNA gene ASV_203, indicating transcriptional activity of lacustrine Crenothrix where it occurred. Another sequence related to lacustrine Crenothrix, aaASV3, correlated with methane, similar to 16S rRNA gene ASV_8 (Figure 6). Overall, the CCA of *pmoA* mRNA aaASVs strengthened the evidence for ecological differentiation of MOB within the oxygen-methane counter gradient.

An additional parsimonious CCA model (Supplementary Figure S3) incorporating further environmental variables suggested that nitrate and sulfate can help explain additional variance in the datasets (total explained variance 65% and 63% 16S rRNA gene and *pmoA* mRNA data, respectively)

on five significant axes. Whereas the variance explained on the first two axes increased only slightly (2.9% and 6%, respectively) and did not reveal fundamentally different aspects of MOB assemblage structure.

Discussion

Our findings suggest that a structured assemblage of different MOB taxa with different ecological niche preferences collectively and effectively performs methane oxidation in stratified lakes (Figure 2, 5). The four lakes harbored both unique and common MOB taxa along the oxygen-methane resource gradient and we discern general patterns of niche preference for some of the common MOB taxa (Figure 6). MOB taxon distributions aligned well with oxygen and methane concentrations, indicating specialization for distinct ecological niches along the counter gradient (Figure 2c).

Main MOB clades of the oxygen-methane counter gradients

In line with previous studies on stratified lakes [21, 51, 52], type Ia MOB dominated the MOB assemblage in terms of diversity and abundance. Different vertical distribution patterns of type Ia MOB taxa, evident from rRNA gene, rRNA and mRNA analysis (Figure 2c, 5b), indicated niche differentiation at a low taxonomic level as suggested in earlier DGGE and cloning-based studies on stratified lakes [5, 21, 22]. In Lake Zug and Lugano another MOB clade, denitrifying *Ca. Methyloirabilis* (NC10 phylum) [11], showed almost equal abundance (Figure 2b), but consisted of only one taxon (ASV_18). Recently, the high abundance and transcriptional activity of this novel candidate species, *Ca. Methyloirabilis limnetica*, have been reported from Lake Zug [10]. We additionally observed *Ca. Methyloirabilis limnetica* in Lake Lugano, suggesting a more important role of these denitrifying MOB in permanently stratified lakes than previously thought.

The three tentative niches correspond to distinct regions of oxygen and methane availability (Figure 1). Oxygen and methane concentrations together with temperature explained up to 47% (CCA of ASVs) of the observed variance. Although other often co-correlated parameters may act as potential co-drivers (C Guggenheim, unpublished), methane and oxygen are obvious drivers constituting the

main growth substrates, which have previously been shown to act selectively on MOB taxa [29, 53]. In the following, we discuss differential distribution patterns and tentative niches of MOB taxa in the oxygen-methane counter gradient from top to bottom with a focus on taxa occurring in more than one lake.

Methane-deficient niche

The methane-deficient niche with increased oxygen concentrations was occupied by ASV_5 of the uncultivated CABC2E06 clade (Figure 2c) and aaASV1 (*pmoA* mRNA) of uncultivated Lake cluster 1 [9], which might stem from the same organism. Although this CABC2E06 sequence has been detected in several aquatic environments [54, 55], its ecology and physiology has so far remained elusive. Our observations allow some hypotheses regarding its ecology to be formulated: to thrive at increased oxygen concentrations requires tolerance for elevated oxygen concentrations as oxygen sensitivity has been shown for some MOB strains [56, 57]. Methane half saturation constants of low affinity MOB are usually $>1\mu\text{M}$ [28] and methane concentrations in the methane-deficient part of the water column are often lower than that, thus a high methane affinity would be advantageous in this habitat. High affinity variants of particulate methane monooxygenase occur in the alphaproteobacterial *Methylocystis*/*Methylosinus* group [58, 59], but also representatives of the upland soil cluster (*Gammaproteobacteria*) have been linked to high-affinity methanotrophy in soils [60]. We speculate that the organism behind the ASV_5/aaASV1 pair has a relatively high methane affinity and tolerates high oxygen concentrations. Confirmation of these traits would, however, require isolation or enrichment. These traits might be shared by other ASVs e.g. ASV_1566 and aaASV22 based on their distribution pattern (Figure 6).

Oxygen-methane interface

The oxygen-methane interface is a narrow zone with potential non-limiting concentrations of both substrates (Rotsee, Figure 2a). MOB with fast growth rates at non-limiting methane and oxygen concentrations could thrive at the interface. The distribution patterns of ASV_166 (related to *Methylomonas*) and aaASV16 (related to *Methylovulum*), both present in Rotsee and Lake Zug, are

congruent with such a niche (Supplementary Figure S5, Figure 5b). Intuitively, one would expect most aerobic MOB to thrive at the oxygen-methane interface, but a pronounced peak of MOB relative abundance at this depth was not observed in the lakes studied (Figure 2b). However, at least in Rotsee and Lake Zug the aerobic MOB assemblage showed maximum potential methane oxidation rates and *pmoA* mRNA copy numbers close to the interface (Figure 5c). Only Rotsee showed a pronounced oxygen-methane overlap at the interface, and only here did we observe ASVs that were strictly confined to the interface. Given this spatial narrowness and lack of a pronounced MOB abundance maximum in this zone in some lakes, it appears likely that much of the methane oxidation takes place above and below the oxygen-methane interface, proceeding under resource-limited conditions. An oxygen-methane overlap might not always be present in stratified lakes [10] due to e.g. significant anaerobic methane oxidation [10] or cryptic oxygen cycling [17, 18, 61] preventing methane from reaching the oxygen gradient. Therefore, this niche might not be present in all lakes or might be temporally restricted. Further, the oxygen-methane interface might be missed by conventional sampling, as it spanned <1 m in case of Rotsee and Greifensee. In the deep lakes where our samples were spaced more widely, we cannot exclude additional fine structure in MOB populations around the interface. However, the gradual depth distributions of many observed taxa did not indicate that we missed important fine structure.

Oxygen-deficient niche

Below the oxygen-methane interface oxygen-deficient conditions with excess methane concentrations appear. Intermittent nanomolar oxygen intrusions can occur, whose depth penetration fluctuates up to several meters within one day [34]. Some MOB are adapted to oxygen deficiency. Two potential pathways, fermentation and denitrification, have been shown to conserve energy in aerobic MOB isolates [24–26]. *Ca. Methyloirabilis oxyfera*-like bacteria, on the other hand, are specifically adapted to anaerobic conditions by generating oxygen internally [11]. Lacustrine *Crenothrix* (ASV_203/aaASV14) preferred the oxygen-deficient part of Lake Zug and Lugano (Figure 2, 5). Lacustrine *Crenothrix* has previously been shown to oxidize methane under

oxygen-deficient conditions and possesses genes for respiratory nitrate reductase and nitrite reductase, which might allow for survival under oxygen-deficient conditions [52]. A closely related sequence, ASV_8 (97% identity to lacustrine Crenothrix), which was present in all lakes investigated and abundant in Rotsee and Greifensee (Supplementary Figure S5), strongly correlated with increased methane concentration (Figure 6). Similarly, aaASV3 correlated with methane and was abundant, confirming transcriptional activity in the oxygen-deficient – high methane part (Figure 6). In line with previous studies [23, 62], MOB affiliated with lineages that are thought to be aerobic abundantly inhabited the oxygen-deficient parts, even in the deep lakes (Lake Zug and Lugano), which remains a puzzling phenomenon [63].

Ca. M. limnetica was most abundant at moderate methane concentrations ($4 \mu\text{mol L}^{-1}$ in Lake Lugano and Zug) under oxygen-deficient conditions (Figure 2c). *Ca. M. limnetica* was absent in Greifensee and Rotsee, which might be due to photosynthetic oxygen production as light penetrates the seemingly anoxic part, likely fuelling aerobic rather than anaerobic methane oxidation [17, 18]. Further, seasonal mixing in Rotsee and Greifensee might limit growth of *Ca. M. limnetica* to months with oxygen-deficient conditions (July – Nov.) [32], which might be too short to compete successfully if doubling times are in the longer range of reported values for *Ca. M. oxyfera* (1 - 2 weeks) [11]. In Greifensee another explanation could be the artificial aeration, which adds oxygen to the hypolimnion [64]. Although Greifensee was oxygen-deficient below 7 m depth according to our measurement, this oxygen source might contribute to the increasing MOB abundance and potential methane oxidation activity with depth (Figure 2a, 5c).

Niche overlap

Although we found compelling evidence for niche partitioning, it is nevertheless evident that the ASVs and aaASVs substantially overlapped along the counter gradient, confirming previous findings [5]. Several ASVs clearly shared each of the described niches; some ASVs show strikingly similar depth distributions (Figure 2d). This raises the question as to which mechanisms allow these organisms to co-occur. As shown previously for Rotsee, Lake Zug and Lugano, the submicromolar

oxygen zone fluctuates in depth, with the highest fluctuations in Lake Zug, spanning between 0.6 to 5.5 m within one day [34]. These fluctuations are faster than estimated environmental MOB growth rates [17], and therefore might allow for species co-occurrence and might blur niche boundaries. To what extent methane concentrations fluctuate is currently unknown as no fast-response sensors are available. An alternative explanation for co-occurrence without competition within the oxygen-deficient part could be anaerobic dormancy [65]. However, in Rotsee, Greifensee and Lake Zug relative MOB abundance, potential methane oxidation rates and *pmoA* mRNA copies were all significantly correlated (Table 1), rather contradicting the dormancy hypothesis. In Lake Lugano, methane oxidation rates did not significantly correlate with MOB relative abundance and *pmoA* mRNA copies, indicating that MOB dormancy may play a role in this system. Alternatively, the lower number of samples in Lake Lugano or other, so far unknown factors may explain the non-significant correlations.

The niche hypothesis based on methane, oxygen and temperature certainly does not explain the entire complexity of our dataset. Some ASVs seem to change niches. For example, ASV_32, occurred in the oxygen-deficient niche in Rotsee and Greifensee, but had a substantial population in the methane-deficient niche and the interface in Lake Zug and Lugano. This could be due to micro-diversity below ASV level (ecotypes) or it could indicate ecological versatility or dependence on other environmental factors not observed in our study. Moreover, we may not always cover the appropriate gradient for each ASV if their main niche was located above or below the investigated counter gradient.

In this study, we have advanced the understanding of distribution, niche partitioning, and the activity of MOB along the oxygen-methane counter gradient of stratified lakes by means of 16S rRNA gene and rRNA, and *pmoA* mRNA analysis, potential methane oxidation rates, and physicochemical measurements at a high vertical profiling and taxonomic resolution. We developed testable hypotheses on niche adaptations of MOB at the ASV level, including a tentative niche for a member of the uncultivated CABC2E06 clade, whose ecology is so far undefined. Future research using

experimental approaches or comparative genomics could yield further insight into potential niche adaptations. We have shown that active MOB populate the oxygen-methane counter gradient and that the MOB assemblage changed from the methane-deficient to the oxygen-deficient part. This leads to the conclusion that the effective methane filter in lakes is structured likely based on niche-specific adaptations. Additionally, we propose that this niche partitioning of MOB could be a mechanism that increases their overall resource exploitation along the oxygen-methane counter gradient, as suggested for other organisms [8]. It is likely that the trait diversity of MOB makes the methane filter in lakes more effective and thus contributes importantly to reducing methane emissions from lakes.

Conflict of interest

The authors declare no conflict of interest.

Acknowledgements

Funding was provided by Swiss National Science Foundation (grant CR23I3_156759). We are grateful to C. Schubert and S. Robert for supporting isotopic analyses. We thank K. Beck, P. Kathriner and C. Dinkel for field and laboratory assistance, and F. Ju, C. Schubert and R. Niederdorfer for helpful comments on the manuscript. Sequencing and data analysis were done in collaboration with the Genetic Diversity Centre (GDC), ETH Zurich.

Supplementary methods and figures are available at the ISME Journal's website.

References

1. Kirschke S, Bousquet P, Ciais P, Saunois M, Canadell JG, Dlugokencky E, et al. Three decades of global methane sources and sinks. *Nat Geosci.* 2013; **6**: 813–823.
2. Bastviken D, Tranvik LJ, Downing JA, Crill PM, Enrich-Prast A. Freshwater methane emissions offset the continental carbon sink. *Science.* 2011; **331**: 50.

- 464 3. Bastviken D, Cole J, Pace M, Tranvik L. Methane emissions from lakes: Dependence of lake
465 characteristics, two regional assessments, and a global estimate. *Global Biogeochem Cycles*.
466 2004; **18**: 1–12.
- 467 4. Conrad R. The global methane cycle: Recent advances in understanding the microbial
468 processes involved. *Environ Microbiol Rep*. 2009; **1**: 285–292.
- 469 5. Biderre-Petit C, Jézéquel D, Dugat-Bony E, Lopes F, Kuever J, Borrel G, et al. Identification of
470 microbial communities involved in the methane cycle of a freshwater meromictic lake. *FEMS*
471 *Microbiol Ecol*. 2011; **77**: 533–545.
- 472 6. Hardin G. The competitive exclusion principle. *Science*. 1960; **131**: 1292–1297.
- 473 7. Levine JM, HilleRisLambers J. The importance of niches for the maintenance of species
474 diversity. *Nature*. 2009; **461**: 254–257.
- 475 8. Finke DL, Snyder WE. Niche partitioning increases resource exploitation by diverse
476 communities. *Science*. 2008; **321**: 1488–1490.
- 477 9. Knief C. Diversity and habitat preferences of cultivated and uncultivated aerobic
478 methanotrophic bacteria evaluated based on pmoA as molecular marker. *Front Microbiol*.
479 2015; **6**: 1–38.
- 480 10. Graf JS, Mayr MJ, Marchant HK, Tienken D, Hach PF, Brand A, et al. Bloom of a denitrifying
481 methanotroph, ‘*Candidatus Methyloirabialis limnetica*’, in a deep stratified lake. *Environ*
482 *Microbiol*. 2018; **20**: 2598–2614.
- 483 11. Ettwig KF, Butler MK, Le Paslier D, Pelletier E, Mangenot S, Kuypers MMM, et al. Nitrite-driven
484 anaerobic methane oxidation by oxygenic bacteria. *Nature*. 2010; **464**: 543–548.
- 485 12. Knittel K, Boetius A. Anaerobic oxidation of methane: progress with an unknown process.
486 *Annu Rev Microbiol*. 2009; **63**: 311–34.
- 487 13. Haroon MF, Hu S, Shi Y, Imelfort M, Keller J, Hugenholtz P, et al. Anaerobic oxidation of

methane coupled to nitrate reduction in a novel archaeal lineage. *Nature*. 2013; **500**: 567–70.

14. Ettwig KF, Zhu B, Speth D, Keltjens JT, Jetten MSM, Kartal B. Archaea catalyze iron-dependent anaerobic oxidation of methane. *Proc Natl Acad Sci*. 2016; **113**: 12792–12796.

15. Weber HS, Habicht KS, Thamdrup B. Anaerobic methanotrophic archaea of the ANME-2d cluster are active in a low-sulfate, iron-rich freshwater sediment. *Front Microbiol*. 2017; **8**: 1–13.

16. Schubert CJ, Vazquez F, Lösekann-Behrens T, Knittel K, Tonolla M, Boetius A. Evidence for anaerobic oxidation of methane in sediments of a freshwater system (Lago di Cadagno). *FEMS Microbiol Ecol*. 2011; **76**: 26–38.

17. Oswald K, Milucka J, Brand A, Littmann S, Wehrli B, Kuypers MMM, et al. Light-dependent aerobic methane oxidation reduces methane emissions from seasonally stratified lakes. *PLoS One*. 2015; **10**: 1–22.

18. Milucka J, Kirf MK, Lu L, Krupke A, Lam P, Littmann S, et al. Methane oxidation coupled to oxygenic photosynthesis in anoxic waters. *ISME J*. 2015; **9**: 1991–2002.

19. Dumont MG, Lüke C, Deng Y, Frenzel P. Classification of pmoA amplicon pyrosequences using BLAST and the lowest common ancestor method in MEGAN. *Front Microbiol*. 2014; **5**: 1–11.

20. McDonald IR, Bodrossy L, Chen Y, Murrell JC. Molecular ecology techniques for the study of aerobic methanotrophs. *Appl Environ Microbiol*. 2008; **74**: 1305–1315.

21. Kojima H, Iwata T, Fukui M. DNA-based analysis of planktonic methanotrophs in a stratified lake. *Freshw Biol*. 2009; **54**: 1501–1509.

22. Tsutsumi M, Iwata T, Kojima H, Fukui M. Spatiotemporal variations in an assemblage of closely related planktonic aerobic methanotrophs. *Freshw Biol*. 2011; **56**: 342–351.

23. Oswald K, Milucka J, Brand A, Hach P, Littmann S, Wehrli B, et al. Aerobic gammaproteobacterial methanotrophs mitigate methane emissions from oxic and anoxic lake

512 waters. *Limnol Oceanogr.* 2016.

513 24. Kalyuzhnaya MG, Yang S, Rozova ON, Smalley NE, Clubb J, Lamb A, et al. Highly efficient
514 methane biocatalysis revealed in a methanotrophic bacterium. *Nat Commun.* 2013; **4**: 2785.

515 25. Kits KD, Campbell DJ, Rosana AR, Stein LY. Diverse electron sources support denitrification
516 under hypoxia in the obligate methanotroph *Methylobacterium album* strain BG8. *Front*
517 *Microbiol.* 2015; **6**: 1–11.

518 26. Kits KD, Klotz MG, Stein LY. Methane oxidation coupled to nitrate reduction under hypoxia by
519 the Gammaproteobacterium *Methylobacterium denitrificans*, sp. nov. type strain FJG1. *Environ*
520 *Microbiol.* 2015; **17**: 3219–3232.

521 27. Hernandez ME, Beck DAC, Lidstrom ME, Chistoserdova L. Oxygen availability is a major factor
522 in determining the composition of microbial communities involved in methane oxidation.
523 *PeerJ.* 2015; **3**: 1–13.

524 28. Knief C, Dunfield PF. Response and adaptation of different methanotrophic bacteria to low
525 methane mixing ratios. *Environ Microbiol.* 2005; **7**: 1307–1317.

526 29. Knief C, Kolb S, Bodelier PLE, Lipski A, Dunfield PF. The active methanotrophic community in
527 hydromorphic soils changes in response to changing methane concentration. *Environ*
528 *Microbiol.* 2006; **8**: 321–333.

529 30. Trotsenko YA, Khmelenina VN. Aerobic methanotrophic bacteria of cold ecosystems. *FEMS*
530 *Microbiol Ecol.* 2005; **53**: 15–26.

531 31. Salcher MM. Same same but different: ecological niche partitioning of planktonic freshwater
532 prokaryotes. *J Limnol.* 2014; **73**: 74–87.

533 32. Schubert CJ, Lucas FS, Durisch-Kaiser E, Stierli R, Diem T, Scheidegger O, et al. Oxidation and
534 emission of methane in a monomictic lake (Rotsee, Switzerland). *Aquat Sci.* 2010; **72**: 455–
535 466.

- 536 33. Odermatt D, Pomati F, Pitarch J, Carpenter J, Kawka M, Schaepman M, et al. MERIS
537 observations of phytoplankton blooms in a stratified eutrophic lake. *Remote Sens Environ.*
538 2012; **126**: 232–239.
- 539 34. Kirf MK, Dinkel C, Schubert CJ, Wehrli B. Submicromolar oxygen profiles at the oxic-anoxic
540 boundary of temperate lakes. *Aquat Geochemistry*. 2014; **20**: 39–57.
- 541 35. Parsons TR, Maita Y, Lalli CM. A manual of chemical and biological methods for seawater
542 analysis, 1st ed. 1984. Pergamon Press, Oxford Oxfordshire.
- 543 36. Holtappels M, Lavik G, Jensen MM, Kuypers MMM. ¹⁵N-labeling experiments to dissect the
544 contributions of heterotrophic denitrification and anammox to nitrogen removal in the OMZ
545 waters of the ocean. *Methods Enzymol*. 2011; **486**: 224–246.
- 546 37. Callahan BJ, Mcmurdie PJ, Rosen MJ, Han AW, Johnson AJ, Holmes SP. DADA2 : High
547 resolution sample inference from amplicon data. *Nat Methods*. 2016; **13**: 581–583.
- 548 38. R Core Team. A language and environment for statistical computing. 2017. Vienna, Austria.
- 549 39. Callahan BJ, McMurdie PJ, Holmes SP. Exact sequence variants should replace operational
550 taxonomic units in marker-gene data analysis. *ISME J*. 2017; **11**: 2639–2643.
- 551 40. Kumar S, Stecher G, Tamura K. MEGA7: Molecular evolutionary genetics analysis version 7.0
552 for bigger datasets. *Mol Biol Evol*. 2016; **33**: 1870–1874.
- 553 41. Quast C, Pruesse E, Yilmaz P, Gerken J, Schweer T, Yarza P, et al. The SILVA ribosomal RNA
554 gene database project: Improved data processing and web-based tools. *Nucleic Acids Res*.
555 2013; **41**: 590–596.
- 556 42. Costello AM, Lidstrom ME. Molecular characterization of functional and phylogenetic genes
557 from natural populations of methanotrophs in lake sediments. *Appl Environ Microbiol*. 1999;
558 **65**: 5066–74.
- 559 43. Henneberger R, Chiri E, Bodelier PLE, Frenzel P, Lüke C, Schroth MH. Field-scale tracking of

560 active methane-oxidizing communities in a landfill cover soil reveals spatial and seasonal
561 variability. *Environ Microbiol.* 2015; **17**: 1721–1737.

562 44. Suzuki R, Shimodaira H. Pvcust: An R package for assessing the uncertainty in hierarchical
563 clustering. *Bioinformatics.* 2006; **22**: 1540–1542.

564 45. Chen H, Boutros PC. VennDiagram: A package for the generation of highly-customizable Venn
565 and Euler diagrams in R. *BMC Bioinformatics.* 2011; **12**: 1–7.

566 46. Benjamini Y, Hochberg Y. Controlling the false discovery rate: a practical and powerful
567 approach to multiple testing. *J R Stat Soc B.* 1995; **57**: 289–300.

568 47. Oksanen J, Blanchet FG, Friendly M, Kindt R, Legendre P, McGlinn D, et al. vegan: community
569 ecology package. R package version 2.5-2. 2018.

570 48. McMurdie PJ, Holmes S. Phyloseq: An R Package for Reproducible Interactive Analysis and
571 Graphics of Microbiome Census Data. *PLoS One.* 2013; **8**: 1–11.

572 49. Deutzmann JS, Stief P, Brandes J, Schink B. Anaerobic methane oxidation coupled to
573 denitrification is the dominant methane sink in a deep lake. *Proc Natl Acad Sci.* 2014; **111**:
574 18273–18278.

575 50. Blazewicz SJ, Barnard RL, Daly RA, Firestone MK. Evaluating rRNA as an indicator of microbial
576 activity in environmental communities: Limitations and uses. *ISME J.* 2013; **7**: 2061–2068.

577 51. Sundh I, Bastviken D, Tranvik LJ. Abundance, activity, and community structure of pelagic
578 methane-oxidizing bacteria in temperate lakes. *Appl Environ Microbiol.* 2005; **71**: 6746–6752.

579 52. Oswald K, Graf JS, Littmann S, Tienken D, Brand A, Wehrli B, et al. Crenothrix are major
580 methane consumers in stratified lakes. *ISME J.* 2017; **11**: 2124–2140.

581 53. Oshkin IY, Beck DAC, Lamb AE, Tchesnokova V, Benuska G, McTaggart TL, et al. Methane-fed
582 microbial microcosms show differential community dynamics and pinpoint taxa involved in
583 communal response. *ISME J.* 2015; **9**: 1119–1129.

- 584 54. Crump BC, Peterson BJ, Raymond PA, Amon RMW, Rinehart A, McClelland JW, et al.
585 Circumpolar synchrony in big river bacterioplankton. *Proc Natl Acad Sci U S A*. 2009; **106**:
586 21208–21212.
- 587 55. Shabarova T, Widmer F, Pernthaler J. Mass effects meet species sorting: transformations of
588 microbial assemblages in epiphreatic subsurface karst water pools. *Environ Microbiol*. 2013;
589 **15**: 2476–88.
- 590 56. Rahalkar M, Bussmann I, Schink B. *Methylosoma difficile* gen. nov., sp. nov., a novel
591 methanotroph enriched by gradient cultivation from littoral sediment of Lake Constance. *Int J*
592 *Syst Evol Microbiol*. 2007; **57**: 1073–1080.
- 593 57. Danilova O V, Suzina NE, Van De Kamp J, Svenning MM, Bodrossy L, Dedysh SN. A new cell
594 morphotype among methane oxidizers: A spiral-shaped obligately microaerophilic
595 methanotroph from northern low-oxygen environments. *ISME J*. 2016; **10**: 2734–2743.
- 596 58. Dunfield PF, Liesack W, Henckel T, Knowles R, Conrad R. High-affinity methane oxidation by a
597 soil enrichment culture containing a type II methanotroph. *Appl Environ Microbiol*. 1999; **65**:
598 1009–1014.
- 599 59. Dam B, Dam S, Kube M, Reinhardt R, Liesack W. Complete genome sequence of *Methylocystis*
600 sp. strain SC2, an aerobic methanotroph with high-affinity methane oxidation potential. *J*
601 *Bacteriol*. 2012; **194**: 6008–6009.
- 602 60. Edwards CR, Onstott TC, Miller JM, Wiggins JB, Wang W, Lee CK, et al. Draft genome sequence
603 of uncultured upland soil cluster Gammaproteobacteria gives molecular insights into high-
604 affinity methanotrophy. *Genome Announc*. 2017; **5**: 1–3.
- 605 61. Garcia-Robledo E, Padilla CC, Aldunate M, Stewart FJ, Ulloa O, Paulmier A, et al. Cryptic
606 oxygen cycling in anoxic marine zones. *Proc Natl Acad Sci*. 2017; **114**: 8319–8324.
- 607 62. Brees J, Niemann H, Wenk CB, Zopfi J, Schubert CJ, Kirf MK, et al. Micro-aerobic bacterial
608 methane oxidation in the chemocline and anoxic water column of deep south-Alpine Lake

- 609 Lugano (Switzerland). *Limnol Oceanogr.* 2014; **59**: 311–324.
- 610 63. Chistoserdova L, Kalyuzhnaya MG. Current Trends in Methylo-trophy. *Trends Microbiol.* 2018;
611 **26**: 703–714.
- 612 64. Wüest A. Belüftung Greifensee im Sommer 2009. *EAWAG Reports.* 2010.
- 613 65. Roslev P, King GM. Aerobic and anaerobic starvation metabolism in methanotrophic bacteria.
614 *Appl Environ Microbiol.* 1995; **61**: 1563–1570.

615 Table legends

616 **Table 1** Spearman correlation coefficients of potential methane oxidation rates and abundance of
617 *pmoA* mRNA/DNA and 16S rRNA/rRNA gene-based relative abundance of methanotrophs for each
618 lake. The *p*-values were corrected for multiple testing (BH), significance is indicated by *p* < .001 ‘***’,
619 *p* < .01 ‘**’, *p* < .05 ‘*’, *p* > .05 ‘not significant (ns)’.

620 Figure legends

621 **Figure 1** Schematic placement of potential MOB niches along the vertical oxygen-methane counter
622 gradient. **a)** Schematic resource gradients of oxygen and methane in proximity to the oxygen-
623 methane interface. **b)** Potential main niches based on resource availability. **c)** Schematic expected
624 distribution patterns of MOB ASVs occupying differential niches.

625 **Figure 2** Vertical distribution patterns of representative methanotrophic 16S rRNA gene ASVs in
626 Rotsee, Greifensee, Lake Zug and Lake Lugano along the oxygen-methane counter gradient. **a)**
627 Chemical profiles. The dashed horizontal line indicates the depth of oxygen depletion to <1 $\mu\text{mol L}^{-1}$.
628 Proposed niches are highlighted in orange, green, gray, and blue. Values below limit of quantification
629 are not shown for CH_4 , NO_3^- , NO_2^- . Note that nitrite was not measured in Lake Lugano. Note that in
630 Greifensee the interface was not sampled, but the position of the niche is indicated. Mind the
631 different y-axis scales for depth (m), and x-axis scales (concentration) for the different lakes. **b)**
632 Proportion of *Methylococcales* and *Ca. Methyloirabilis limnetica* of bacterial 16S rRNA gene

sequences. **c)** The most abundant ASV from each cluster in **d)** is depicted, representing the distribution of the respective cluster. On top, the maximum relative abundance of each ASV compared to all bacterial 16S rRNA gene sequences is shown. Colors are ASV-specific. **d)** Cluster analysis based on Pearson's distance of the depth distribution patterns of relative abundance of MOB 16S rRNA gene ASVs. Dark grey boxes depict clusters identified. The scale shows the Pearson's distance. Raw data of *Ca. M. limnetica* relative abundances, nitrate and methane data in Lake Zug have been used for a previously published figure in the supporting information [10].

Figure 3 Venn diagrams showing number of shared **a)** MOB ASVs based on the 16S rRNA gene and **b)** amino acid ASVs based on *pmoA* mRNA between the four lakes: R=Rotsee, G=Greifensee, L=Lake Lugano, Z=Lake Zug. ASV and aaASV identities are listed in boxes, which are colored accordingly.

Figure 4 Neighbor joining tree of methanotroph 16S rRNA gene ASVs and *pmoA* mRNA aaASVs retrieved from the oxygen-methane counter gradients of Rotsee, Greifensee, Lake Zug and Lake Lugano. **a)** Partial 16S rRNA gene sequences (423bp) were used to calculate a tree with the Neighbor-Joining method using Jukes-Cantor evolutionary distance. **b)** Partial *pmoA* amino acid sequences (155 positions) were used to calculate a tree with the Neighbor-Joining method using the Poisson correction. Nodes with bootstrap values >0.7 (10000 replicates) are highlighted with a black circle. Accession numbers of reference sequences are to the left of their names. The scale bars (bottom) display changes per nucleotide or amino acid position.

Figure 5 Vertical profiles of representative *pmoA* mRNA aaASVs in Rotsee, Greifensee, Lake Zug and Lake Lugano along the oxygen-methane counter gradient. **a)** Cluster analysis based on Pearson's distance of relative abundance patterns of the *pmoA* mRNA aaASVs (unique amino acid *pmoA* sequences), which clusters aaASVs with similar depth distribution. Dark grey boxes depict the identified clusters. **b)** The most abundant aaASV from each cluster is depicted representing the distribution of the respective cluster. On top, the maximum relative abundance of each aaASV compared to all *pmoA* mRNA sequences is shown. Colors are aaASV specific and highlight the most

658 abundant aaASV of each cluster in a). c) Corresponding profiles of *pmoA* mRNA copies L⁻¹ determined
659 by qPCR and potential methane oxidation rates (MOX) derived from ¹³C-CH₄ incubations are shown.
660 The dashed line indicates oxygen depletion to <1 μmol L⁻¹. Tentative main niches are highlighted in
661 orange, green, gray and blue (see Figure 1 and Results). Mind the different scales of the axes
662 between lakes.

663 **Figure 6** Canonical correspondence analysis (CCA) calculated based on a Chi-square dissimilarity
664 matrix using relative abundances compared to all MOB sequences in a sample (sample sum=1) and
665 physicochemical parameters (T=temperature). The CCA was calculated for **a)** 16S rRNA gene MOB
666 ASVs and **b)** *pmoA* mRNA aaASVs in 65 samples from the oxygen-methane counter gradient of the
667 four different lakes. Colors are ASV/aaASV specific and correspond to the colors used in previous
668 figures. The dot size visualizes the number of lakes in which the ASV/aaASV occurred.

Table 1

Spearman's rho	Rotsee (n=18)				Greifensee (n=19)			
	1.	2.	3.	4.	1.	2.	3.	4.
1. CH ₄ -ox. rate (μmol L ⁻¹)								
2. <i>pmoA</i> mRNA (copies L ⁻¹)	0.77 ***				0.74 ***			
3. <i>pmoA</i> DNA (copies L ⁻¹)	0.67 **	0.74 ***			0.59 **	0.74 ***		
4. MOB 16S rRNA rel. ab.	0.66 **	0.75 ***	0.67 **		0.85 ***	0.70 ***	0.72 ***	
5. MOB 16S rRNA gene rel. ab.	0.86 ***	0.77 ***	0.62 **	0.73 ***	0.91 ***	0.75 ***	0.71 ***	0.95 ***

Spearman's rho	Lake Zug (n=17)				Lake Lugano (n=10-11)			
	1.	2.	3.	4.	1.	2.	3.	4.
1. CH ₄ -ox. rate (μmol L ⁻¹)								
2. <i>pmoA</i> mRNA (copies L ⁻¹)	0.62 *				0.36 ns			
3. <i>pmoA</i> DNA (copies L ⁻¹)	0.36 ns	0.69 **			0.67 ns	0.70 ns		
4. MOB 16S rRNA rel. ab.	0.94 ***	0.66 **	0.44 ns		0.31 ns	0.93 ***	0.65 ns	
5. MOB 16S rRNA gene rel. ab.	0.95 ***	0.69 **	0.48 ns	0.95 ***	0.36 ns	0.95 ***	0.67 ns	0.99 ***

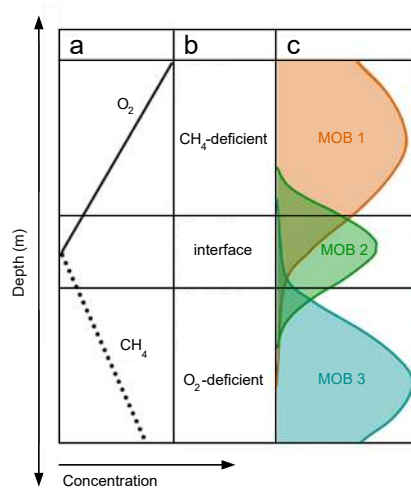


Figure 1

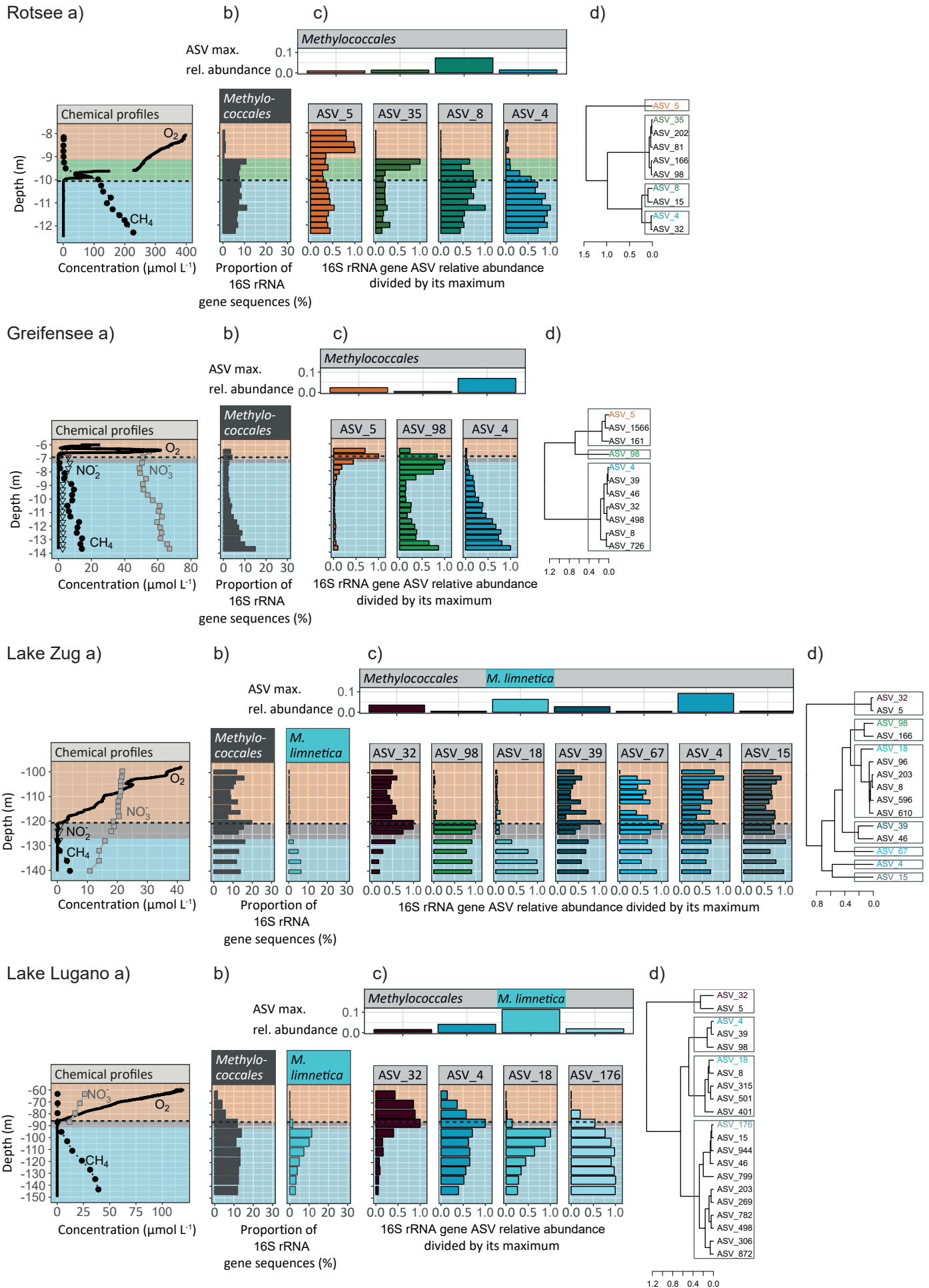
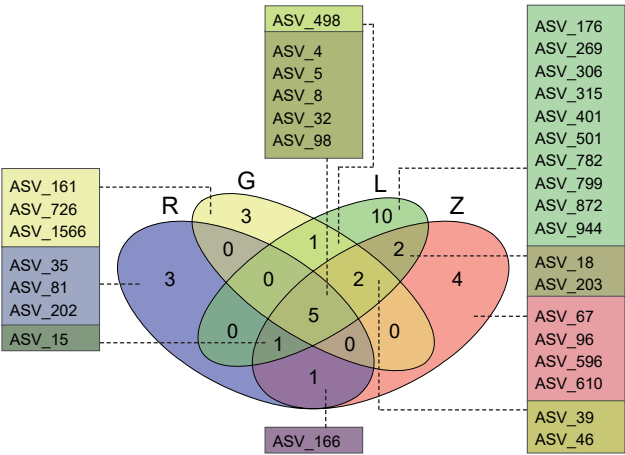


Figure 2

a) Venn diagram: 16S rRNA gene ASVs



b) Venn diagram: *pmoA* mRNA aaASVs

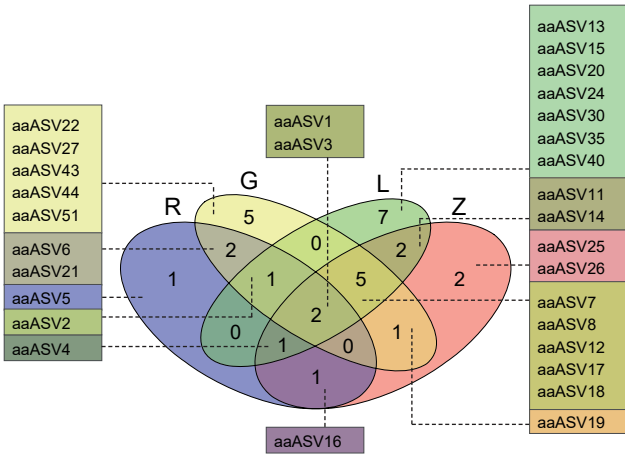
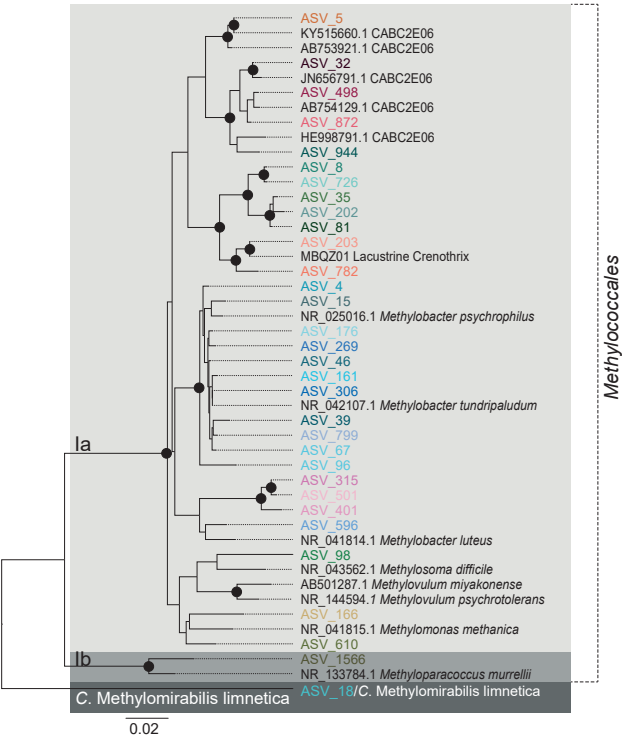


Figure 3

a) 16S rRNA gene NJ tree



b) *pmoA* mRNA NJ tree

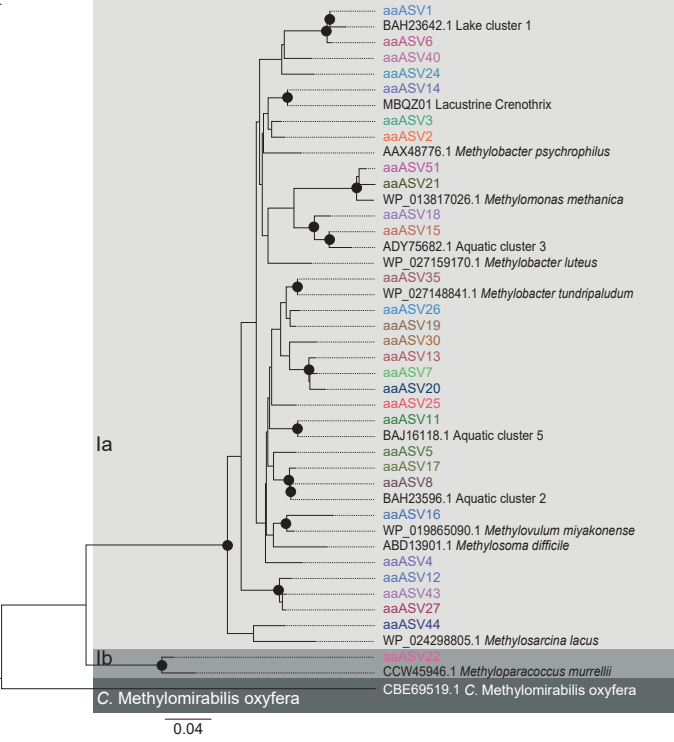


Figure 4

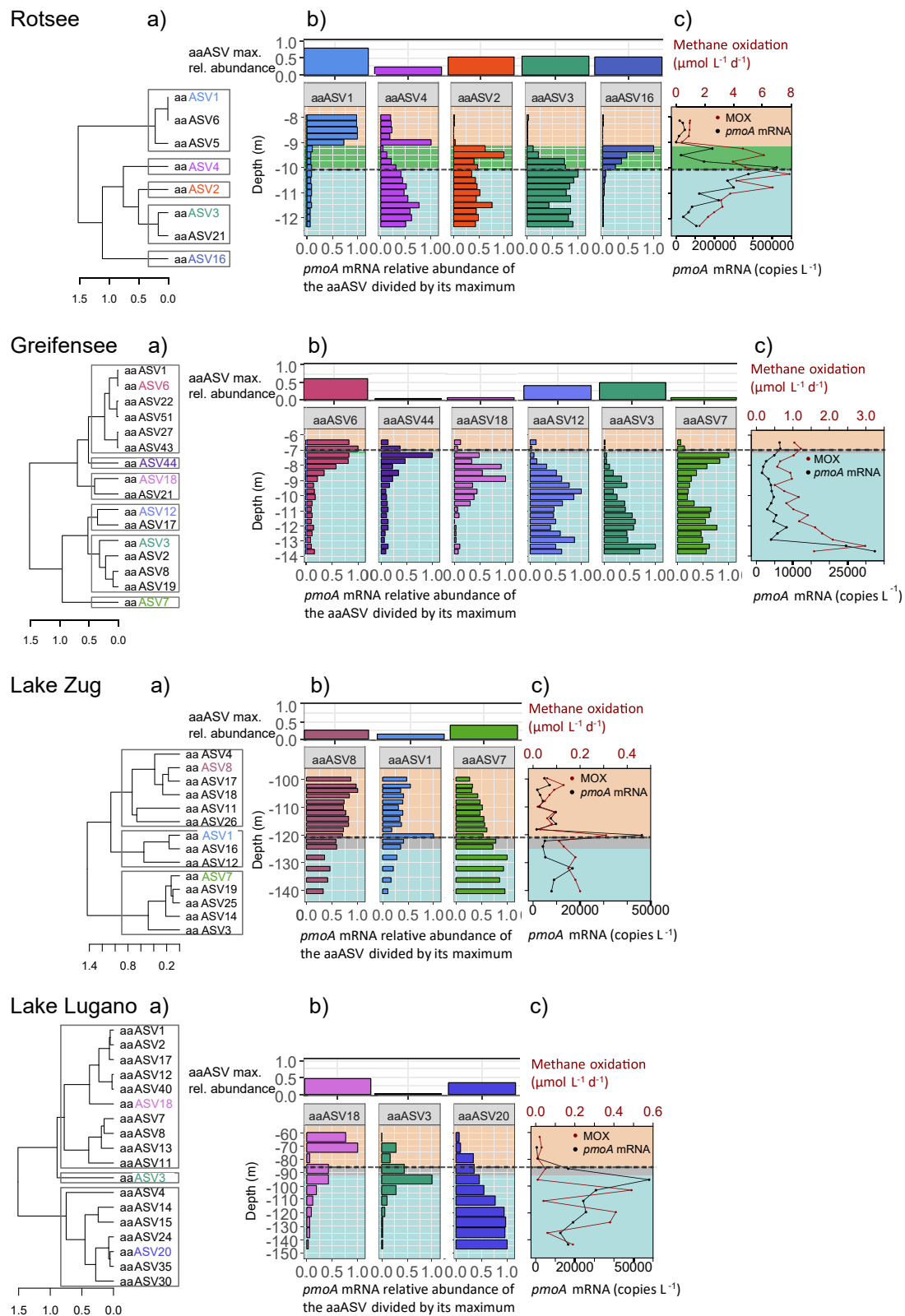


Figure 5

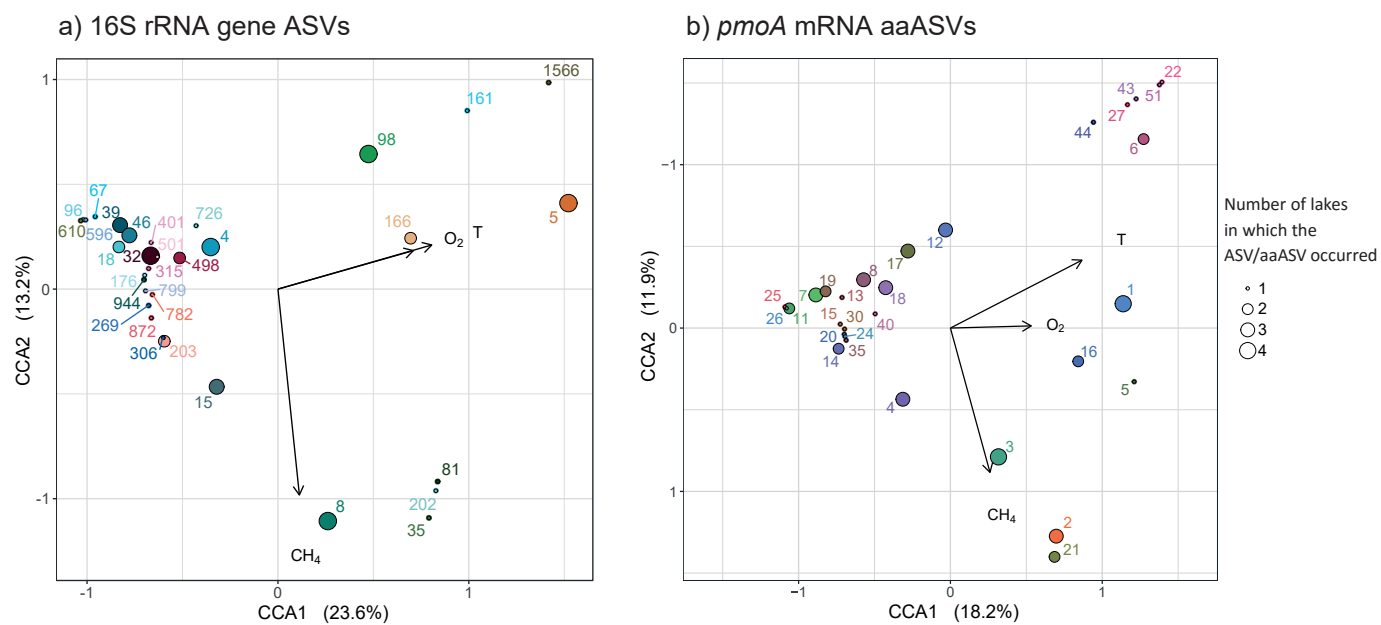


Figure 6